STUDIES OF PHOBOS' ORBIT, ROTATION, AND SHAPE USING SPACECRAFT IMAGE DATA

K. Willner, J. Oberst, B. Giese, M. Wählisch, K-D. Matz, T. Roatsch, H. Hoffmann

German Aerospace Center
Institute of Planetary Research, Planetary Geodesy
Runtherfordstr. 2, 12489 Berlin, Germany
- konrad.willner@dlr.de
http://www.dlr.de/pf

Commission IV, WG IV/7

KEY WORDS: Phobos, Control Point Network, Shape, Orbit Model, Astrometric Observations

ABSTRACT:

Images obtained by the High Resolution Stereo Camera (HRSC) and the Super Resolution Channel (SRC) on the European Mars Express (MEX) spacecraft have renewed the interest in Phobos, the larger of the two Martian satellites. We are involved in a comprehensive study in geodesy and cartography of this small irregular (13.4 x 11.2 x 9.2 km) satellite. We focus on astrometric measurements to refine and validate the current Phobos orbit models, on an update of the Phobos control point network to study rotational and global shape parameters, and a global Digital Terrain Model in high resolution.

1. INTRODUCTION

In 1877 Asaph Hall, an astronomer at the United States Naval Observatory, discovered the Martian moons Phobos and Deimos. Phobos, the larger of the two moons, is orbiting with a mean distance of 9375 km to the center of Mars, deep in the gravitational field of the planet. Hence, Phobos' long term orbital evolution may reveal constraints on the elastic properties of the Martian interior. Up to the current date Phobos' orbit is being studied by means of ground-based observations during Mars oppositions on a several kilometers accuracy level (Morley, 1989, Veiga, submitted). Mariner 9 obtained the first spacecraft images of Phobos, which were used to determine Phobos' position with an accuracy of 3 to 10 km (Duxbury and Callahan, 1989a). Further observations by the Viking orbiters led to similar accuracies for positional observations (Duxbury and Callahan, 1988) as well as to a control point network (Duxbury and Callahan, 1989b) and shape and surface models (Duxbury, 1991). In 1989, the Russian Phobos 2 Mission made 37 positional observations of Phobos with an estimated accuracy of 2 km (Kolyuka et al., 1991). A decade later, MGS (Mars Global Surveyor) revisited Phobos. MOLA (Mars Orbiter Laser Altimeter) range measurements to Phobos (Banerdt and Neumann, 1999) and positional observations of Phobos' shadow (Neumann et al., 2004) were carried out. With the observation of Phobos eclipse events from the Mars Exploration Rovers, discrepancies of 12 km to the orbit prediction models were reported (Bell et al., 2005). These discrepancies were later confirmed by a number of flyby observations obtained by the SRC on Mars Express (MEX) (Oberst et al., 2006). Motivated by the large number of new observations and the uncertainties of orbit data, JPL (Jacobson and Rush, 2006) and ROB (Lainey et al., 2007) released new orbit models. Studying the geodesy and cartography of Phobos we validated available orbit prediction models by means of comparison with new SRC flyby observations. Furthermore an independent and global control point network was determined on the basis of SRC and Viking Orbiter image data. The control point network is used to study

rotational parameters of Phobos and will be used to derive physical parameters such as volume and bulk density of Phobos.

2. MARS EXPRESS PHOBOS FLYBYS AND SRC IMAGING

Mars Express is orbiting Mars in a highly elliptical nearly polar orbit. With an apoapsis of near 10,000 km, the orbit is reaching well beyond the nearly circular and equatorial Phobos orbit with a mean radius of 9375 km. As the orbit periods of MEX and Phobos are similar, there are usually epochs of close Phobos encounters in consecutive flybys followed by periods with no close Phobos approaches (Oberst et al., 2008). The SRC is used to obtain high resolution images of Phobos during close flyby encounters. Owing to its large focal length of 988.5 mm, images resolve with 10 m/pxl at a distance of 1000 km. Until April 2008 a total of 92 successful flyby maneuvers were performed, from which image data were returned. The mean flyby distance of orbits where useful SRC images were obtained is at about 2000 km (with a minimum range to Phobos of 590 km and a maximum range of 11,000 km). Hence, image resolutions vary between 5 m/pxl and 100 m/pxl but are mainly better than 20 m/pxl (see Figures 1 and 2). For a detailed description of the camera and MEX orbital parameters see (Oberst et al., 2008) and (Jaumann et al., 2007), respectively.

3. ORBIT VALIDATION

3.1 Flyby sequences

During a Phobos flyby, the camera systems are pointed at one fixed inertial point in the celestial sphere. The HRSC needs to operate at least one line sensor due to technical constraints but usually scans the sky for Phobos with several line sensors for stereo imaging. In addition, a sequence of 8 SRC images is obtained during one flyby. The first and the last SRC images of

one sequence are dedicated to long exposures to observe faint background stars with visual magnitudes of m = 4 to 9, which are used to control the camera pointing.

3.2 Camera Pointing

Camera pointing uncertainties have a major influence on the accuracy of astrometric measurements. Long-time exposure images containing background stars were taken during almost all Phobos flybys since mid 2005. Stars are usually observed just before and after a Phobos encounter, giving us the opportunity to control/correct predicted pointing information and check for possible pointing drifts during the flyby. In cases in which just one star was observed, we assumed that a twist angle with respect to the nominal orientation information is negligible. This was later confirmed by the reduction of the observations (cf. Section 3.4). To control the camera pointing

we compute image coordinates of stars from star catalogs (ESA, 1997, Röser and Bastian, 1992) applying nominal pointing information and compare these with the observed line/sample coordinates of the stars. Differences between the star positions are interpreted as pointing displacement. Hence, all further observations of the flyby are corrected accordingly. In general the nominal pointing information for the SRC is in good agreement with the observed positions of the stars and within the accuracy constraints set by the initial specifications for spacecraft orientation. Nevertheless, four outliers were found in orbits 682, 2706, 2739 and 4568 where discrepancies between predicted and observed star positions of up to 450 SRC pixels were observed. During one image sequence the pointing remains very stable. The average difference between the first and the last image of a flyby sequence is 8 pixels which relates to 0.004 degree.
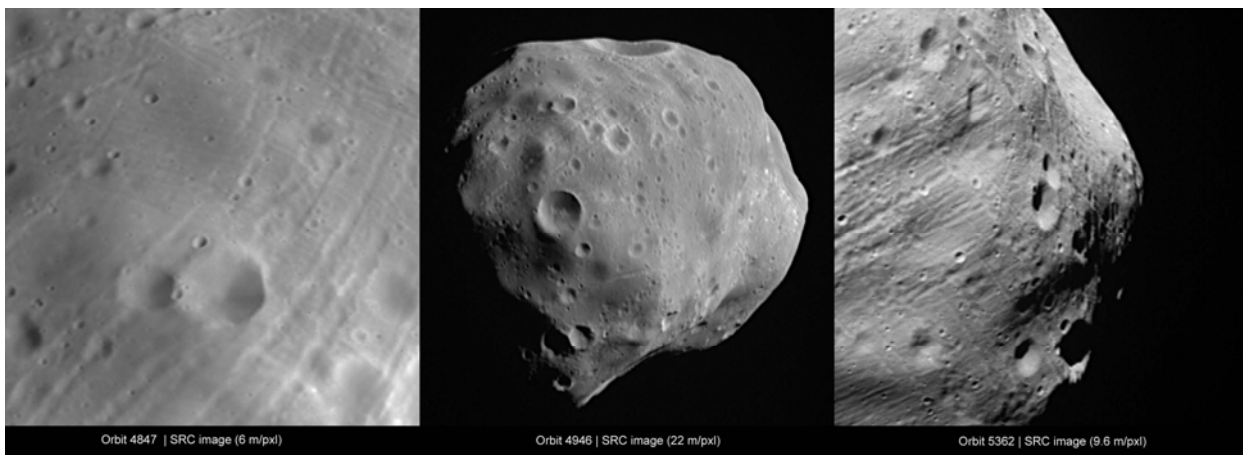
Figure 1: Examples of recent flyby images obtained by the SRC with different flyby distances

3.3 Astrometric Measurements

While our previous analysis (Oberst et al., 2006) was based on fitting an ellipsoidal model to the observed limb of Phobos, we further improved our method by making use of a control point network (Duxbury and Callahan, 1989a, Duxbury, 1991). The 3-D Cartesian coordinates of 315 control points, all of them craters, some very large, are given with respect to the center of mass of Phobos. The control points are identified in the SRC images and line/sample coordinate pairs are measured. These points are defined as the center of a crater on the mean local surface (Duxbury and Callahan, 1989b). As craters are typically observed from quite different viewing angles, much effort was made to consistently measure their image coordinates. Points on the crater rim were collected and an ellipse fit method was applied to reconstruct the center of the crater on the level of the crater rim. On average 9, but a minimum of 3, surface features were identified and measured in each image. Using the Phobos orbit model, the corrected camera pointing and the Phobos-fixed coordinates of the craters, we computed the predicted image coordinates of the control points. To fit the observed image coordinates, the predicted line/sample pairs of the control points were transformed. An iterative least-squares adjustment was used to solve for the unknown transformation parameters, rotation, scale and 2 translations. To derive information on the position of the COM (center of mass) of Phobos, we then computed the predicted line/sample coordinates of the the COM for the specific image and applied the previously determined transformation parameter.

3.4 Results

By April 2008, over 280 SRC images were obtained during 92 successful flyby maneuvers. As some images suffer from smear, lack of identifiable control points, insufficient surface coverage, or lack of background star observations, we considered 120 images from 51 orbits for the analysis. For these images the iterative least-squares analysis to determine the transformation parameters converged rapidly. Results indicated that both, the scale factor and rotation parameter, are negligible for the transformation leaving translations in line and sample direction between the predicted and observed image coordinate sets. We studied the translation vectors in the object space, especially in along-track and across-track direction (radial to the central body or out of the orbit plane) for the two recently released orbit models (Jacobson and Rush, 2006, Lainey et al., 2007). While no significant across-track offsets were found, small along-track offsets between orbit prediction models and our observations remain, ranging from 1.5 km to 2.6 km, depending on the orbit model used (Willner et al., submitted). Phobos' positions were observed with an estimated accuracy of ±0.1km to ±0.5km depending on the flyby distance. Comparing observed Phobos' position with orbit predictions, both models show the same discrepancy pattern, whereas differences to the orbit prediction by Jacobson and Rush, (2006) are larger by approx 35%
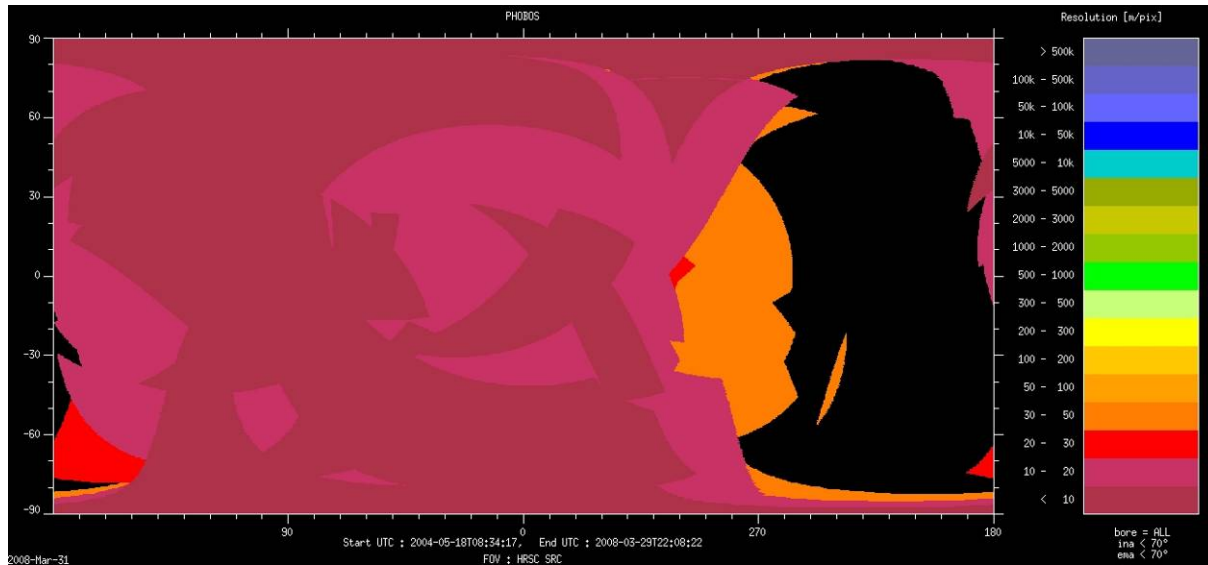
Figure 2: Equidistant map of current surface coverage of SRC images on Phobos.

4. CONTROL POINT NETWORK

4.1 Duxbury and Callahan control point network

The Viking orbiters were the first to obtain complete ground coverage of Phobos with excellent phase angle coverage. Pixel resolutions of the images are in the order of 200 m or better. The first global control point network consisted of 98 points (Duxbury and Callahan, 1989b), mostly craters. It was later extended to over 315 control points. The measurements included relatively large craters covering several pixels. Uncertainties of the 3D-coordinates of the points ranged from ±74 m to ±900 m (Duxbury, 1991).

4.2 HRSC and SRC image data

The resolution of HRSC images from a range of 2000 km is approx. 80 m. Hence, though the built-in stereo capability seem to make the HRSC attractive for control point network analysis, only a limited number of HRSC images from more or less 10 flyby maneuvers would be suitable for an in depth control point network analysis.

For SRC on the other hand, with its large focal length of 988.5 mm, the ground pixel size is smaller by a factor of approx. 4.3 over that of HRSC. Pixel resolutions of SRC images for flybys range from 100 m/pxl to 5m/pxl. The back draw in case of SRC image data is, that SRC is a single frame camera, pointed to a fixed point in the stellar sky during one flyby. Thus, the same surface area needs to be observed during different flybys with different viewing angles to be useful for photogrammetric techniques. The establishment of an independent control point network for Phobos requires a global image coverage. HRSC and SRC images cover approx. 74% of Phobos' surface in stereo (cf. Figure 2). Viking orbiter images were incorporated into the image database to fill the gap on the anti-Mars side of Phobos. Fortunately very high resolution images, of the missing area, are available in the Viking data set.

4.3 Object point determination

We measured line/sample coordinates of control points in 53 SRC images and 16 Viking orbiter images. Contrary to Duxbury and Callahan (1989b) our control points are defined as the centers of a crater on the crater floor. Since image resolutions allow us to observe very small surface features – even small features within large craters – we assume that the surface features are shallow and represent a mean surface to sufficient approximation. A total of 660 points were observed 3845 times with a minimum of 2 observations and a maximum of 14 observations, but on average 6 observations per point in both image data sets.

Initially the two sets of observations – SRC images and Viking orbiter images – were processed separately to control the predicted orientation information. Nominal navigation data for the SRC images could directly be used to determine object point coordinates of the control points in a least-squares bundle block adjustment. For a few orbits, normalized residual values of the camera orientation data indicated that uncertainties of the position and pointing observations were larger than expected. An adopted weighting scheme for observed camera orientations was applied to reduce the relevance of uncertain observations on the adjustment. Estimating that image coordinates were observed with a 1 pixel uncertainty, mean object point accuracies σ_x, σ_y, σ_z of 39.6 m, 34.6 m, and 36.1 m, respectively, were computed, for control points measured in SRC images.

	SRC	Viking orbiter
No. of points obs.	2953	871
σ_{max} [m]	92.1	164.2
σ_{min} [m]	32.7	91.7
σ_{mean} [m]	36.8	100.9
Combined Adjustment of SRC and Viking		
No. of points obs.	3841	
σ_{max} [m]	62.5	
σ_{min} [m]	4.4	
σ_{mean} [m]	15.9	

Table 3: Object point accuracies for the different bundle block adjustment models.
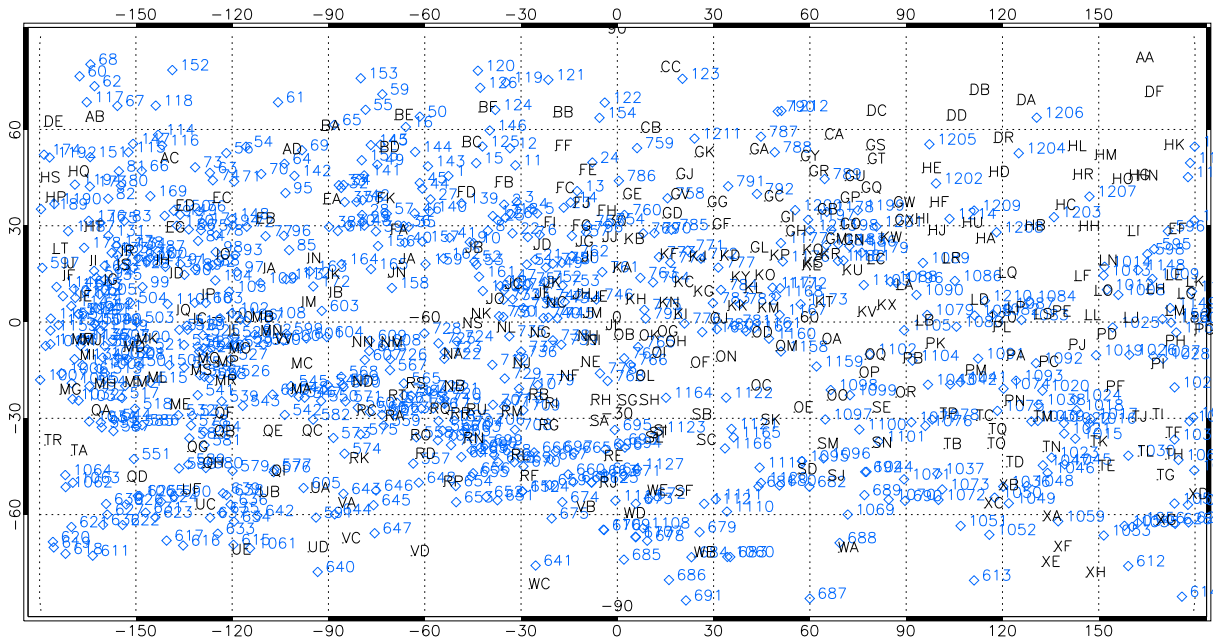
Figure 4: Control points (blue) of the DLR network in comparison with the Duxbury and Callahan control point network (letters). The density has increased by a factor of two while the uncertainty of the control point coordinates is approx. a 6 times lower.

To successfully compute a block adjustment with Viking orbiter data, navigation information needed to be improved prior to the computation. Therefore, we improved the pointing information by fitting the predicted limb position in the image to the observed figure. For images with very high resolution – showing only parts of the surface but not the limb of Phobos – an overlay of the Duxbury and Callahan control points was produced and moved to fit to surface features in the image to improve the camera orientation. To further optimize results, accuracy values for orientation data were adjusted according to the computed normalized residuals. Overall, a bundle block adjustment with Viking orbiter data was very sensitive to variations in the stochastic model. Object points were determined with uncertainties σ_x, σ_y, σz of 111 m , 90 m, 101 m when a measurement accuracy of 1 pixel was assumed.

For the computation of a global control network both data sets were combined through conjugate points in overlapping areas. Since reduction of the Viking orbiter image measurements was very dependent on the stochastic model chosen Viking image orientations were introduced as unknown parameters rather than additional observed values. The computed spacecraft orientations for MEX and the Viking orbiters were then used to determine the object point coordinates of the control points in a second run. Furthermore, a Baarda gross error detection (Baarda, 1968) was applied to remove misidentified measurements. Thus, uncertainties of the 3D ground coordinates could significantly be reduced by a factor of 3 for points in SRC images and a factor of approx. 6 for points in Viking images (cf. Tabel 3).

4.4 Global Shape

Control points are irregularly distributed over the surface of Phobos (see Figure 4). To determine the shape of Phobos a triangulation between the points was computed. A few gross errors remain in the coordinates of the control points,

represented by artifacts. Even though the distribution of the 660 control points is quite irregular (Figure 4) the network is a good basis for a global shape model, which shows many details such as of medium sized craters. A preliminary version of the shape model is shown in Figure 5.

4.5 Rotation Parameter

For the reduction of the control point network, nominal values of unknown parameters of the bundle block adjustment are computed with respect to the body centered, body fixed, coordinate frame. Thus, a different orientation of the observed body may lead to a solution with reduced stresses in the network as the nominal camera orientations – acting as unknowns and observed parameters in the adjustment – do change with the orientation of the body. This situation is exploited to observe rotational parameters of Phobos.

Even though Phobos is in a synchronous orbit around Mars, a free libration can be observed due to the varying angular speeds along an elliptical orbit. Furthermore, Phobos' pronounced non-spherical body interacts with the gravitational field of Mars causing a forced libration, a superimposed sinusoidal oscillation.

We concentrated on the observation of the forced libration amplitude from the control point network. The least-squares adjustment of the control point network was computed for a varying forced libration amplituds. Subsequent studies of the residuals of the control
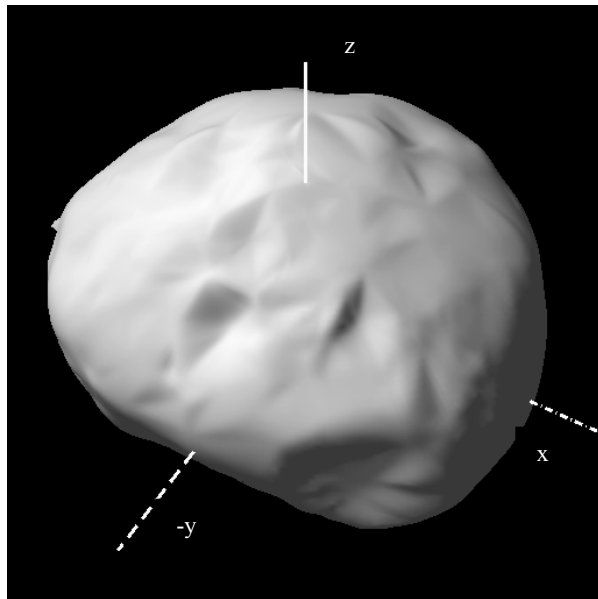
(a) Phobos' leading side
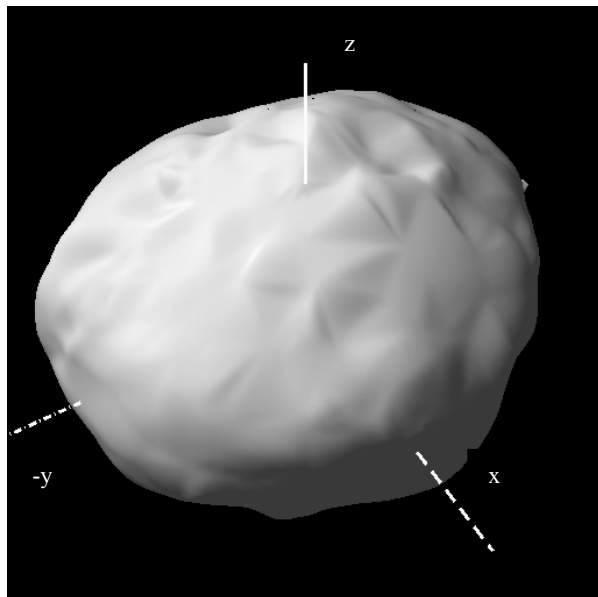
(b) Phobos' trailing side

Figure 5: Shape model from triangulation of the control point network. The x-axis (dot-dash) points towards Mars, the y-axis (long-dashed) points in the direction of motion and the z-axis marks the rotation axis. Note that the y-axis in Figure 5(a) points in the direction of motion and is in the negative y direction of the IAU frame. In Figure 5(b) the positiv y-axis is displayed
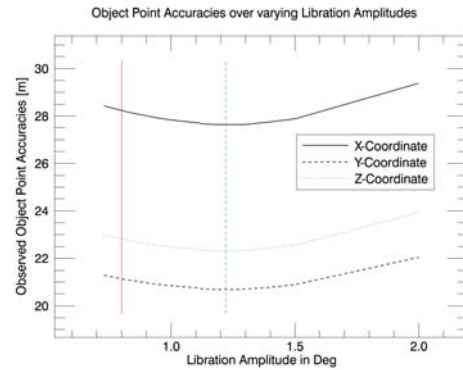
Figure 6: Observed residuals of object points for varying forced libration amplitudes. The red vertical line indicates the observation by (Duxbury, 1991) , the green line indicates the minimum of SRC observations.

points, indicate an amplitude of 1.2° for the force libration (see Figure 6). The observed amplitude differs slightly from the amplitude of $0.80 \pm 0.3°$ observed and computed by (Duxbury and Callahan, 1988, Duxbury, 1991), but is in well agreement with the amplitude of 1.2° derived from a topographic model (Borderies and Yoder, 1990). The topographic model of the later reference was approximated through a Kriging interpolation of the 98 control points from the 1989 control point network (Duxbury, 1989). A correction for the Stickney crater was made in the topography model. A deviation of the forced libration amplitude from previous observed amplitudes could have its cause in the mass distribution model. Current studies assume a homogeneous mass distribution for Phobos. Mass concentrations could significantly change inertia figures which can be related to the forced libration amplitude in a first approximation. Equation (1) shows this relation, where θ_A is the forced libration amplitude, e equals the excentricity of Phobos, and $A \leq B \leq C$ are the moments of inertia.

$$\gamma = \frac{B-A}{C} \qquad \theta_A = \frac{2e}{1-\frac{1}{3}\gamma} \qquad (1)$$

5. CONCLUSIONS AND FUTURE WORK

We observed Phobos' positions over a three year time span through astrometric measurements in SRC image data. A new reduction method was established which can be applied to any planetary body and may prove to be useful for analysis of future planetary data sets. The ongoing MEX mission with further close flyby maneuvers will make more observations available, adding constraints to the Phobos orbit models.

The control point network was primarily used to observe the forced libration amplitude. Estimates of the volume and moment of inertia factors are yet to come, and may further constrain the bulk density and mass distribution of Phobos.

Currently, studies of HRSC stereo data are under way to derive a global digital terrain model (DTM) in high resolution. A DTM derived from Viking orbiter images will be needed to fill the unobserved area on the anti-Mars side of Phobos.

REFERENCES

Baarda, W., 1968. A testing procedure for use in Geodetic networks. Publications on Geodesy, New Series, Vol. 2 Number 5, Netherlands Geodetic Commission, Rijkscommissie voor Geodesie, Kanaalweg 4, Delft, Netherlands.

Banerdt, W. B. and Neumann, G. A., 1999. The Topography (and Ephemeris) of PHOBOS from MOLA Ranging. In: Lunar and Planetary Institute Conference Abstracts, pp. 2021–+.

Bell, J. F., Lemmon, M. T., Duxbury, T. C., Hubbard, M. Y. H., Wolff, M. J., Squyres, S. W., Craig, L. and Ludwinski, J. M., 2005.Solar eclipses of Phobos and Deimos observed from the surface of Mars. Nature, 436, pp. 55–57.

Borderies, N. and Yoder, C. F., 1990. Phobos' gravity field and its influence on its orbit and physical librations. A&A, 233, pp. 235–251.

Duxbury, T. C., 1989. The figure of PHOBOS. Icarus, 78, pp. 169–180.

Duxbury, T. C., 1991. An analytic model for the PHOBOS surface. Planetary and Space Science, 39, pp. 355–376.

Duxbury, T. C. and Callahan, J. D., 1988. PHOBOS and Deimos astrometric observations from Viking. A&A, 201, pp. 169–176.

Duxbury, T. C. and Callahan, J. D., 1989a. PHOBOS and Deimos astrometric observations from Mariner 9. A&A, 216, pp. 284–293.

Duxbury, T. C. and Callahan, J. D., 1989b. PHOBOS and Deimos control networks. Icarus, 77, pp. 275–286.

ESA, 1997. The Hipparcos and Tycho Catalogues (ESA 1997). VizieR Online Data Catalog, 1239, pp. 0–+.

Jacobson, R. A. and Rush, B., 2006. Ephemerides of the martian satellites -mar063. JPL IOM 343R-06-004.

Jaumann, R., Neukum, G., Behnke, T., Duxbury, T. C., Eichentopf, K., Flohrer, J., Gasselt, S. v., Giese, B., Gwinner, K., Hauber,E., Hoffmann, H., Hoffmeister, A., Köhler, U., Matz, K.-D., McCord, T. B., Mertens, V., Oberst, J., Pischel, R., Reiss, D., Ress, E., Roatsch, T., Saiger, P., Scholten, F., Schwarz, G., Stephan, K. and Wählisch, M., 2007. The high-resolution stereo camera (HRSC) experiment on Mars Express: Instrument aspects and experiment conduct from interplanetary cruise through the nominal mission., Planetary and Space Science, 55, pp. 928–952.

Kolyuka, Y., Tikhonov, V., Ivanov, N., Polyakov, V., Avanesov, G., Heifetz, V., Zhukov, B., Akim, E., Stepanyants, V., Papkov, O. and Duxbury, T., 1991. PHOBOS and Deimos astrometric observations from the PHOBOS mission. A&A, 244, pp. 236–241

Lainey, V., Dehant, V. and Pätzold, M., 2007. First numerical ephemerides of the Martian moons. A&A, 465, pp. 1075–1084.

Morley, T. A., 1989. A catalogue of ground-based astrometric observations of the Martian satellites, 1877-1982. Astronomy and Astrophysics Supplement Series, 77, pp. 209–226.

Neumann, G. A., Bills, B. G., Smith, D. E. and Zuber, M. T., 2004. Refinement of Phobos Ephemeris Using Mars Orbiter Laser Altimeter Radiometry. In: S. Mackwell and E. Stansbery (eds), Lunar and Planetary Institute Conference Abstracts, pp. 1820–+.

Oberst, J., Matz, K. D., Roatsch, T., Giese, B., Hoffmann, H., Duxbury, T. and Neukum, G., 2006. Astrometric observations of Phobos and Deimos with the SRC on Mars Express. A&A, 447, pp. 1145–1151.

Oberst, J., Schwarz, G., Behnke, T., Hoffmann, H., Matz, K.-D., Flohrer, J., Hirsch, H., Roatsch, T., Scholten, F., Hauber, E., Brinkmann, B., Jaumann, R., Williams, D., Kirk, R., Duxbury, T., Leu, C. and Neukum, G., 2008. The imaging performance of the SRC on Mars Express. Planetary and Space Science, 56, pp. 473–491.

Röser, S. and Bastian, U., 1992. The final PPM star catalogue for both hemispheres. Bulletin d'Information du Centre de Donnees Stellaires, 42, pp. 11–16.

Veiga, C. H., submitted. Phobos and Deimos' CCD observations.

Willner, K., Oberst, J., Wählisch, M., Matz, K.-D.and Roatsch, T., Jaumann, R. and Mertens, V., submitted. New astrometric observations of Phobos with the SRC on Mars Express.